RELATIONSHIP BETWEEN PETROGRAPHIC PORE TYPES AND CORE MEASUREMENTS IN SANDSTONES OF THE MONSERRATE FORMATION, UPPER MAGDALENA VALLEY, COLOMBIA

R. EHRLICH ‡, G. COBALEDA*, and J. BARCLAY FERM ◊

‡ Energy and Geosciences Institute, University of Utah, Salt Lake City, Utah, USA
◊ Perception and Decisions Systems, Inc. Columbia, South Carolina, USA
Ecopetrol - Instituto Colombiano del Petróleo, A.A. 4185 Bucaramanga, Santander, Colombia
e-mail: gcobaleda@infantas.ecp.com

Patterns of porosity in sandstones of the Monserrate Formation (Upper Magdalena Valley) exposed in polished blocks have been digitally recorded using an image processor coupled to a scanning electron microscope operated in backscatter electron mode. Additionally, porosity, permeability and response to mercury injection-capillary pressure tests were measured on some of the imaged samples. Porosity patterns were evaluated via an erosion/dilation-differencing image-processing algorithm and then classified by the self-training classifier, SAWVEC. Changes in the resulting pore type proportions were strongly associated with changes in the mercury porosimetry curves. From the image processing data, five pore types, sufficient to include all of the variability in size and shape of the patterns of porosity, were identified. Variations in the number of pores of each type per unit cross sectional area were related to variations in permeability. The resultant relationships with mercury porosimetry demonstrated that pores of the same type tend to form microcircuits characterized by a limited throat size range. Permeability modeling showed that intergranular Pore Types 2 and 4 (secondary porosity resulting from carbonate dissolution) are responsible for permeability in the 0,01 - 0,10 Darcy range. Type 5 pores (large molds) slightly contribute to permeability, except in coarse grained rocks where they are efficiently connected by microfractures.

Patrones de porosidad de areniscas pertenecientes a la Formación Monserrate (Valle Superior del Magdalena), expuestos sobre bloques pulidos, fueron capturados y digitalizados mediante procesador de imágenes acoplado al Microscopio Electrónico de Barrido operado en detección de electrones retrodispersos. Adicionalmente se midieron la porosidad y permeabilidad, y se realizó porosimetría de mercurio. Los patrones de porosidad se evaluaron por algoritmos de procesamiento que hacen uso de diferenciación vía erosión/dilatación, y posteriormente fueron clasificados mediante el programa SAWVEC. A partir del procesamiento se establecieron cinco tipos de poro, suficientes para describir toda la variabilidad en tamaño y forma del espacio poral en estudio. Variaciones en el número de poros de cada tipo por unidad de área transversal se relacionaron con la permeabilidad. La relación resultante con la porosimetría de mercurio demostró que poros de un mismo tipo tienden a formar microcircuitos caracterizados por un tamaño de garganta restringido. El modelo de permeabilidad demostró que los poros intergranulares tipo 2 y 4 (porosidad regenerada a partir de disolución de carbonatos) son los responsables del flujo en el rango de 0,01 a 0,10 Darcy. Poros tipo 5 (móldicos de gran tamaño) sólo contribuyen a la permeabilidad en muestras de grano grueso, donde se encuentran eficientemente conectados mediante microfracturas.

Keywords: *Monserrate Formation, sandstones, permeability, microfracturing, image analysis, pore types, Hg porosimetry*

* *A quien debe ser enviada la correspondencia*

INTRODUCCION

Productivity of many reservoir sandstones is related to the nuances of the spatial distribution of porosity rather than the amount of porosity. For instance, in Colombia, reservoirs with as little as 10 percent porosity, can carry more permeability than sandstones with twice that porosity. In this paper, the results of a pilot study to determine the controls on permeability in the Monserrate Formation of the Upper Magdalena Valley are discussed. Most of the samples have low (< 0,01 Darcy) to intermediate (0,01 - 0,10 Darcy) values of permeability, but some are much more permeable. In this investigation, image analysis of porosity is linked with core analysis (permeability and the results of mercury porosimetry), as a guide leading to the understanding of the petrology of enhanced permeability.

Ehrlich *et al.* (1991a, b) showed, using Petrographic Image Analytical (PIA) procedures and physical models, that only a fraction of the total porosity controls permeability and many other physical properties of reservoirs. PIA methodology establishes an objec-tive procedure to take digitized images of porosity quantify the size and shape of pores, and classify those pores into pores types. The PIA metodology also establishes the relative proportion of each pore type per sample. Finally, Ehrlich's methodology uses a version of the Hagen-Poiseuille capillary tube law to model permeability. McCreesh *et al.* (1991) showed that specific pore types are correlated with different pressure intervals of mercury capillary pressure curves when pore types are derived from end cuts of the plugs used in mercury porosimetry. This study showed that pores of the same type tend to be connected to each other, forming microcircuits. Experience has shown that this is broadly correct for relationships between samples taken from the same reservoir within an oil field, however; the assumption can be tested by examining deviations from regression and sensitivity analysis based on inclusion or deletion of individual samples from the analysis. Graton and Fraser (1935) predicted that "packing flaws" in sandstones would form circuits composed of oversized pores connected by oversized pore throats and that these circuits would be the primary flow carriers in unconsolidated sands. Prince *et al.* (1995), using Fourier analysis, demonstrated the existence of such circuits in quartz-rich reservoir sandstones.

Packing flaws are not the unique features that can enhance permeability. Fracture systems, natural and induced, are commonly recognized as important factors in the increased mobility of fluids. Many fracture systems enhance productivity for a relatively short time because they represent limited storage capacity and, after initial high production rates, production declines as the porous interfracture matrix begins to control permeability. The time span between fracture flow and interfracture matrix flow is a function of the surface area of the fracture and the number of intersections between the fracture surface and the interfracture matrix porosity The pore typing procedure, when applied to the samples of Monserrate Formation, resulted in the identification of a previously undescribed kind of microfracture that is both permeability-enhancing and apparently has large amounts of storage capacity.

James, R. A. (1995) investigated a Devonian reservoir sandstone in the Kane Field of Pennsylvania which shares some characteristics with the Upper Magdalena Monserrate Formation. The Kane field is also characterized by low porosity (< 10 per cent) and low permeability (< 0,010 Darcy). This sandstone has produced oil for more than fifty years and has responded well to waterflooding. This is truly an unconventional behavior considering that relative permeabilities should be much lower than the measured single phase values. The analysis of thin sections carried out by James, R. A. (1959) showed that enhanced permeability (and injectivity) was controlled by a single oversized pore type (one to three grain diameters long and about one to two grain diameters wide). That pore type also controlled most of the storage capacity of the rock; that is, samples that contained little or none of this pore type had low porosity and the lowest values of permeability. Correlating the pore type information with mercury porosimetry data showed that porosity associated with this oversized pore type contributed an order of magnitude more permeability to total flow than typical porosity associated with packing flaws. Conventional petrographic classification would define this pore type from its visual appearance as either: a) a mold, b) a dissolution of early, patchy carbonate cement, or c) an artifact of coring or thin section preparation. The combination of the image data with the mercury porosimetry and permeability

measurements suggested that none of these possibilities were probable. Similar pore types have also been detected in many other reservoirs, including Miocene sandstones from the Gulf of Thailand (Bowers *et al.*, 1994) and in several other reservoirs in South America. Examination under cathodoluminescence of these pores, in one of the latter reservoirs, showed that it is interconnected by microcracks produced by the expansion of the sandstone fabric, connecting pores into a permeable network. This sort of microfracturing commonly occurs in foreland fold belts or areas subjected to transpression.

In summary, the combination of image analysis and core physics can quantitatively determine the physical relevance of pore types to flow characteristics. Rock sections provide information on porosity exposed on the surface of a plane, while core analyses quantify the physical properties of a small volume. If physical properties increase or decrease as one or more pore types increase or decrease in abundance, then there would be a relationship between the plane of section and the physical properties of the three dimensional pore complex. Other properties correlated with pore types could include S_{wi}, S_{or} (Ehrlich *et al.*, 1997), NMR response (Bowers *et al.*, 1995; Carr *et al.*, 1996), fracture toughness (Ferm *et al.*, 1990), and electrical conductivity (Ehrlich *et al.*, 1991b).

METHODS

Experimental

The initial investigation involved analysis of 32 samples taken from cores of three wells penetrating the Monserrate Formation located in the Dina field, Upper Magdalena Valley in Colombia. The sandstone is of Cretaceous (Maestrichtian/Campanian) age. The samples covered virtually the entire sand size and texture range. Quartz is the dominant framework mineral. The samples covered the range of effective porosity and air permeability previously measured for routine analysis of the field.

End cuts from the samples plugs were impregnated with epoxy resin, then polished and coated with carbon for image acquisition using an image analyzer: a C-Imaging 1.280, coupled to a Cambridge Instruments S240 Scanning Electron Microscope (SEM), operated in backscatter electron detection mode (BSE). Twenty-five images per sample were taken at 120x magnification. Each rectangular field of view represents an area of approximately 1 mm^2. In addition, thin sections were prepared for conventional petrography using the transmitted light petrographic microscope.

Based on image processing results, as well as on prior knowledge of porosity and permeability results, a subset of samples was chosen on which additional physical measurements and mercury porosimetry were performed using the sample plug remainder. Effective porosity and permeability were measured with an automated core measurement system, CMS200, with the API RP40 procedure. Mercury injection was performed, in the range of 0 to 60.000 psi, using an ICP proprietary procedure in a Micromeritcs Autopore 9220.

Image Acquisition and Processing.

Binary images (pore versus matrix) were produced by thresholding the gray scale BSE-SEM images. The size and shape of porosity elements were measured using the Perception and Decision Systems' erosion/dilation program. Data from all of the fields of view of each sample were pooled into a spectrum of smooth/rough areas (Ehrlich *et al.*, 1984, 1991a). The smooth/rough spectrum represents a frequency distribution of the scales of roughness of the porosity elements, as well as the distribution of sizes of essentially the largest inscribed circle in each of the porosity elements. Each sample was represented by a spectrum containing data from fifty-five cycles of erosion/dilation. The raw data were combined into "bins" conforming to maximum entropy criteria (Full *et al.*, 1984), in order to ensure maximum unbiased contrast between samples.

Derivation of Pore types

After binning, the data were represented by a matrix of fifteen columns (the maximum entropy smooth/rough areas). Three parameters were then determined: 1) the number of pore types, using SAWVECA, 2) The smooth/rough spectrum of each pore type, and 3) the relative proportions of each pore type in each sample. The number of pore types equals the number of significant eigenvectors that can be derived from the data matrix via singular value decomposition. One of the criteria for determining this is the precision by which the raw data can be back-calculated from an incom-

plete set of eigenvectors.

Once the number (n) of pore types had been determined, the pore type spectra and relative proportions were determined iteratively using the program SAWVECB. Each pore type, represented by a smooth/rough area spectrum containing non-negative elements, can be considered to occupy a vertex of a n-1 dimensional polyhedron (a n-1 dimensional simplex). Accordingly, all samples can be considered as linear combinations spectra of the vertices and, by virtue of the geometry, the sum of coefficients associated with each pore type in each sample equals unity. Thus, the coefficients represent relative proportions.

Mercury Porosimetry and Porosity - Permeability Modeling

A regression based procedure (McCreesh *et al.*, 1991) was applied to the pore type proportions and the mercury porosimetry data. The regression analysis yielded "pore type coefficients" which represent the proportion of each pore type being filled in each pressure interval. With each pore type associated with a pressure range, a throat size for each pore type could then be calculated. Once calculated via regression the pore type throat sizes could be tested against a permeability model based on the Hagen-Poisueille version of Darcy´s law (Ehrlich *et al.*, 1991b). In this model, permeability is a function of the number of pores of each type per cross-sectional unit area and throat size of each pore type raised to the fourth power. The average throat size is determined from the regression procedure and the number of pores of a given pore type is determined from pore type proportions, pixel size and total optical porosity (TOP).

ANALYSIS AND DISCUSSION OF RESULTS

Five pore types are sufficient to describe the variability of porosity observed in the samples. These five pore types are each represented by a spectrum of smooth/rough areas. Samples rich in one or another pore type were examined and images representing each pore type were selected (Figure 1). Pore type proportions, characteristic grain size, TOP, porosity and physically measured permeability are presented in Table 1 and the number of pore types per unit area for each sample are presented in Table 2.

Pore Type 1

Pore Type 1 (the smallest pore type) has an average width of 5,4 μm and represents residual porosity remaining after almost complete occlusion of intergranular porosity, commonly by quartz overgrowths, incomplete carbonate cementation, or pressure solution. Pore Type 1 tends to be most abundant in the finer grained sandstones which also have low values of optical porosity (<10%) even though physically measured porosity may be as high as 15 per cent (Table 1). Many of the samples are bioturbated resulting in a patchy fabric consisting of an array of coarse- and fine-grained patches resulting in poor sorting at a larger scale, but well-sorted on a small scale. Type 1 pores are more common in the finer grained patches. Significant amounts (10% - 30%) of Pore Type 1 can also occur at other grain sizes. In coarser grained rocks, Pore Type 1 characterizes large patches (tens of grains across) wherein intergranular porosity has been destroyed by overgrowth development or pressure solution. Pore Type 1 appears as small discrete pores in the plane of section, indicating that its associated pore throats are so small that they are seldom if ever intersected by the plane of the section.

Pore Type 3

Pore Type 3 has a relatively narrow width (13 μm), but has an intricate shape. It is a type of intragranular porosity developed within micaceous/argillaceous rock fragments. Pores of this type are represented in section as thin tortuous pores within these rock fragments.

Pore Types 2 and 4

Pore Types 2 (11 μm wide) and 4 (23 μm wide) seem to be variations on a single theme. Each pore type tends to be most abundant at a different grain size: Pore Type 2 in fine-to-medium grained rocks, Pore Type 4 in medium-to-coarse grained rocks. These pore types appear to be the result of the dissolution of intergranular carbonate cement.

Pore Type 5

Pore Type 5 is abundant in only seven of the 32 samples. These samples are coarse-grained and include the samples with the highest permeability. Type 5 pores are large (grain size or larger, averaging 62 μm wide)

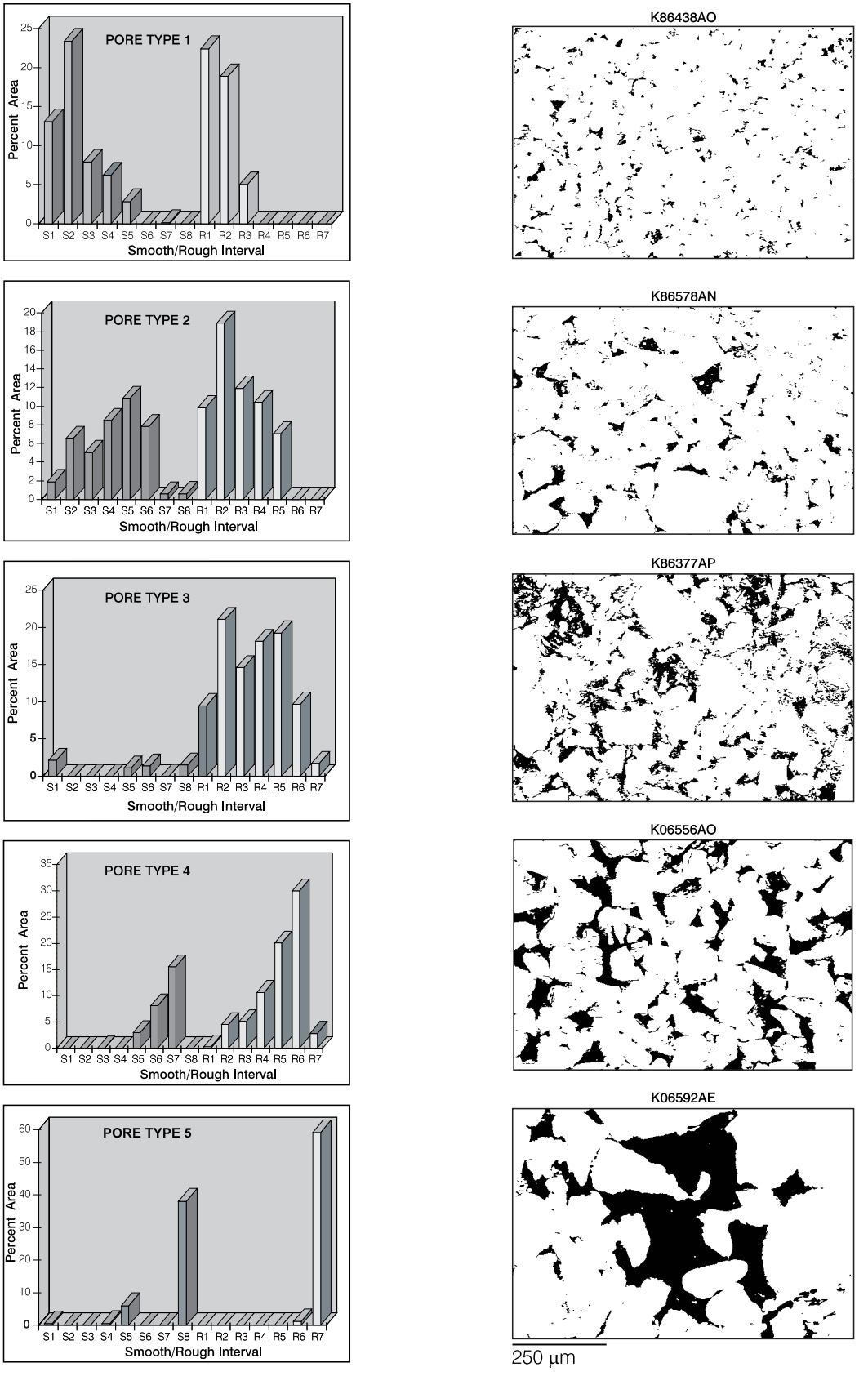

Figure 1. Representative images of each of five Pore Types and the erosion/dilation spectra that define them.

Table 1. Basic Statistics.

BASIC PORE TYPE STATISTICS									
SAMPLE	GR. SIZE	%PT1	%PT2	%PT3	%PT4	%PT5	POROSITY	TOP	PERM
D36380	MGr	,47,98	20,23	20,33	8,64	2,83	13,1	9,26	4,30
D36410	CGR	11,71	30,62	31,06	26,62	0,00	3,7	13,16	214
D36450	FGR	57,32	37,00	5,51	0,17	0,00	19,6	10,37	15,5
D36474	FGR	73,61	19,98	2,23	3,78	0,40	16,4	6,43	15,7
D36500	CGR	22,46	0,72	18,54	39,27	19,02	18,2	10	378
D36530	CGR	22,07	36,07	23,79	16,25	1,82	15	8,58	26,1
D36610	FGR	17,47	52,96	23,51	6,05	0,00	19	15,3	52,5
D36646	MGR	5,15	42,84	8,74	37,45	5,82	19	14,4	77,9
D36702	MGR	40,34	33,18	11,70	14,77	0,00	15	7,68	3,03
K06556	MGR	10,80	16,79	0,31	66,37	5,73	17,7	16,24	106
K06573	CGR	9,45	50,17	8,44	31,95	0,00	16	8,78	83,9
K06592	CGR	11,36	0,00	3,65	36,02	48,97	16,8	16,27	107
K06628	FGR	65,51	27,13	4,32	3,03	0,00	17,2	7,03	6,63
K06649	CGR	19,71	1,81	9,42	21,76	47,30	8,4	10,65	2,56
K06672	CGR	12,01	11,09	20,76	47,67	8,46	13	9,07	25,3
K06712	CGR	18,02	15,91	22,73	39,21	4,12	14,1	10,58	25,1
K06725	CGR	13,49	41,80	6,32	33,60	4,79	12	8,63	23,1
K06730	CGR	24,03	57,13	11,17	7,59	0,08	15,7	12,14	11,5
K06737	MGR	38,85	5,89	15,70	17,00	22,56	10,7	9,4	1,69
K06757	FGR	0,00	60,54	13,43	26,03	0,00	16,5	14,84	32,7
K26725	CGR	4,32	34,79	19,30	38,82	2,78	16,4	12,11	119
K86377	MGR	18,27	52,50	29,12	0,00	0,11		13,23	
K86402	MGR	5,44	49,79	19,69	25,07	0,00		13,23	
K86409	FGR	39,45	53,55	7,00	0,00	0,00	16,1	9,42	9,75
K86438	FGR	76,02	20,55	1,41	2,02	0,00	17,1	6,45	8,54
K86471	CGR	18,35	0,00	10,41	50,59	20,65	11,9	11,02	22,5
K86494	CGR	10,33	28,58	8,16	47,33	5,59	13,7	9,26	33
K86521	CGR	9,50	3,62	18,68	52,93	15,27	17,1	12,59	177
K86535	MGR	0,00	11,27	33,71	32,84	22,18	12,5	13,56	13,2
K86551	MGR	4,74	52,13	13,78	26,98	2,37	12,9	8,64	6,71
K86578	FGR	0,00	84,52	4,15	11,33	0,00	15,8	9,5	39,4
K86582	FGR	27,55	60,13	12,32	0,00	0,00	14,3	10,35	16,4

(C: Coarse, M: Medium, F: Fine)

Table 2. The number of pores per square mm for each Pore Type

PORE NUMBER STATISTICS						
SAMPLE	GR. SIZE	NP1/sq. mm	NP2/sq. mm	NP3/sq. mm	NP4/sq. mm	NP4/sq. mm
D36380	MGR	737,38	46,39	1,62	2,70	0,20
D36410	CGR	255,69	99,77	3,52	11,82	0,00
D36450	FGR	986,32	94,99	0,49	0,06	0,00
D36474	FGR	784,80	31,78	0,12	0,82	0,02
D36500	CGR	372,56	1,78	1,60	13,24	1,44
D36530	CGR	314,16	76,60	1,76	4,70	0,12
D36610	FGR	443,66	200,61	3,10	3,12	0,00
D36646	MGR	123,05	152,71	1,08	18,19	0,63
D36702	MGR	514,14	63,08	0,77	3,83	0,00
K06556	MGR	290,96	67,48	0,04	36,36	0,70
K06573	CGR	137,63	109,00	0,64	9,46	0,00
K06592	CGR	306,59	0,00	0,51	19,77	6,03
K06628	FGR	763,83	47,20	0,26	0,72	0,00
K06649	CGR	348,41	4,77	0,87	7,82	3,81
K06672	CGR	180,78	24,91	1,62	14,59	0,58
K06712	CGR	316,40	41,68	2,07	14,00	0,33
K06725	CGR	193,23	89,33	0,47	9,78	0,31
K06730	CGR	484,05	171,67	1,17	3,11	0,01
K06737	MGR	606,14	13,71	1,27	5,39	1,60
K06757	FGR	0,00	222,47	1,72	13,04	0,00
K26725	CGR	86,78	104,26	2,01	15,85	0,25
K86377	MGR	400,89	171,88	3,32	0,00	0,01
K86402	MGR	119,43	163,06	2,25	11,19	0,00
K86409	FGR	616,71	124,89	0,57	0,00	0,00
K86438	FGR	813,25	32,79	0,08	0,44	0,00
K86471	CGR	335,57	0,00	0,99	18,81	1,72
K86494	CGR	158,79	65,55	0,65	14,79	0,39
K86521	CGR	198,53	11,29	2,03	22,49	1,45
K86535	MGR	0,00	37,82	3,94	15,02	2,27
K86551	MGR	67,93	111,46	1,03	7,86	0,15
K86578	FGR	0,00	198,85	0,34	3,63	0,00
K86582	FGR	473,17	154,05	1,10	0,00	0,00

and appear to be molds produced by dissolution of a fine-grained rock fragment, probably a fine-grained volcanic.

Relationship between Pore Types and Throat Size

Mercury injection porosimetry is a rich source of information concerning the configuration of porosity. Mercury is an intensely non-wetting phase for all reservoir rocks and will not spontaneously enter the rock (imbibe). It can enter into rock only by being forced in under pressure. Commonly, mercury intrudes the rock at some value of pressure (entry pressure) and only fills circuits defined by the largest pore throats. After entry, increasing pressure will ultimately result in the invasion of all the porosity, with mercury flowing through the smallest pore throats and the nooks and crannies of pores at the highest pressures. The product of a mercury injection test is a curve that records the proportion of porosity filled as a function of pressure. Making relatively minor assumptions (because mercury is so intensely non-wetting), throat size can be related to pressure; thus the mercury injection curve tells us how much porosity is located behind throats of certain sizes.

If pores of each type were randomly placed relative to one another, there would be very low probability for the existence of long circuits consisting of pores of a single type. If, on the other hand, there exists a relationship between pore type and throat size and pores of a given type tend to form circuits, then one should observe a relationship between mercury saturation at various pressure intervals and pore type proportions.

In the case of the Monserrate samples, the relationship between pore type and throat size is similar among all samples, except for the most permeable ones. This exception is of course, extremely important with respect to reservoir production. The relationships between pore types and throat size are summarized in Table 3, prediction coefficients represent the proportion of each pore type which fills at each pressure interval. The precision of the estimation of saturation versus pressure, based on the regression equations, can be seen in Figure 2. The filling pattern at the highest pressures (> ~10.000 psi, related to the smallest throat size) is probably more due to the filling in of corners and pore wall irregularities than to entry into throats less than about 0,01 μm.

Four of the five pore types display a uniform rela-

Table 3. Mercury injection prediction equations.

Radius (μm)	Pressure (psi)	BASIC PORE TYPE STATISTICS					
		%PT1	%PT2	%PT3	%PT4	%PT5	%PT5'
106,7 - 35,6	0 - 3	0	0	0	0	0	0
35,6 - 11,9	3 - 9	0	0	0	0	0	0
11,9 - 8,2	9 - 13	0	0	0	3,67	0	100
8,2 - 4,6	13 - 23	0	0	0	77,86	0	0
4,6 - 3,0	23 - 35	0	28,64	0	15,92	0	0
3,0 - 1,8	35 - 60	0	30,01	16,75	0	20,24	0
1,8 - 1,1	60 - 95	27,47	8,69	5,72	0	16,81	0
1,1 - 0,43	95 - 250	29,98	9,52	17,57	0	15,63	0
0,43 - 0,089	250 - 1200	22,18	12,26	23,90	0	12,53	0
0,089 - 0,0097	1200 - 11,000	12,05	5,03	19,10	0	12,53	0
< 0,0097	11,000 - 60,000	8,32	5,86	16,96	2,55	22,27	0
		100	100	100	100	100	100

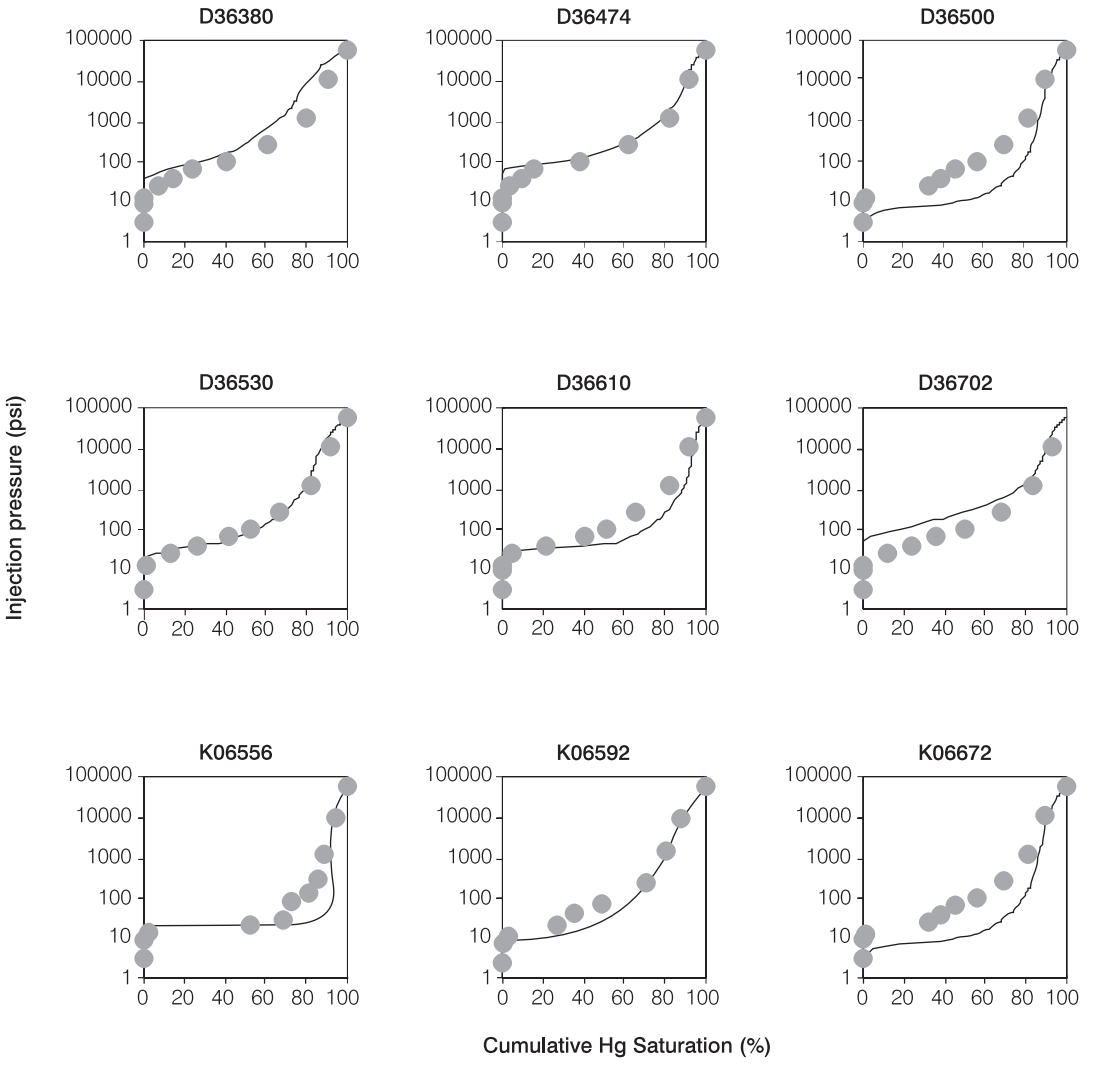

Figure 2. Predicted (dots) and measured (solid line) mercury injection curves

tionship between pore type and throat size. Pore Type 1 is entered in the pressure range of 60 - 95 psi (throats of 1 - 2 μm) and most of the pores of this type are entered at pressures corresponding to a throat size of about 1 μm. Pores of this type are associated with such small throats that they cannot contribute much to permeability and are probably associated with bound or irreducible water (S_{wi}).

Pore Type 2 fills over a pressure range of 23 - 60 psi and is characterized by throats in the range of about 3 - 4 μm. Although the throat size is relatively small, it will be shown that Pore Type 2, by virtue of its abundance, is a major supporter of permeability in the range of 0,001 - 0,050 Darcy.

Pore Type 3, the intragranular pore type, is associated with throats averaging 1 μm or less. The small throat size and the fact that this porosity is localized as discrete patches within the pore complex insures Pore Type 3 contributes little to permeability and is likely to contain irreducible fluids (S_{wi}).

Pore Type 4 fills at the 13 - 25 psi range and is characterized by throats of 5 - 8 μm. When abundant, Pore Type 4 can be a significant contributor to enhanced permeability. Pore Type 5 is the major exception to the assumption of a uniform relationship between pore types and throat size across all samples. When the highest permeability samples (> 0,1 D) are excluded from the regression analysis, Pore Type 5 is

characterized by throats of about 2μm and therefore begins filling at about 50 psi. When these samples are included, the regression indicates two modes of filling; one in the pressure interval 9 - 13 psi (throats ranging from 8 to 12mm) and then a resumption of filling as calculated from the data set when the high permeability samples were removed. Unfortunately, there were not enough high permeability samples to run a separate regression.

This pattern of selective filling shows that the Monserrate sandstones possess circuits consisting of pores of the same type juxtaposed and connected by throats of a restricted size range.

Permeability

Pores comprise the porosity of a rock but, themselves, do not contribute to permeability. Instead, flow is sensitive to the ways in which pores are mutually connected, the sizes of the pore throats and the association between pore types and throat size. A permeability model is a way to relate the throat size information derived from the discussion above to permeability. The main use of the model is to determine the influence of each pore type on the permeability of each sample. Assuming that all pores have about the same number of pore throats, then permeability should be proportional to the number of pores of each type and the characteristic throat size of each pore type.

The Monserrate samples vary in permeability from 0,00169 to 0,378 Darcy. On the basis of simple visual inspection, the samples can be classified into coarse-(coarse-to-very coarse sand), medium, and fine-grained (fine-grained sand-to-coarse silt) categories. Guided by the relationships between pore types and mercury porosimetry, the ways in which permeability is partitioned between pore types can be investigated. The validity of the exercise can then be evaluated in a separate exercise where the entry pressure of the mercury injection tests is estimated, based on pore type information and permeability values.

In the hagen-Poiseulle model, permeability is related to throat size to the fourth power. Therefore, larger throats have a disproportionate effect on permeability. The converse is also true, pores connected by very small throats cannot make much of a contribution to permeability. If one hypothesizes that Pore Type 1 (1 μm throats) influences permeability, one can test it by observing the sensitivity of permeability to the abundance of Pore Type 1 by postulating larger and larger throat sizes and observing the result. Can a significant permeability be achieved from Pore Type 1 and still be in accord with the capillary pressure data? The answer is no. Pore Type 1 fails, depending on the sample, by: a) not producing significant model permeability unless it is assigned a throat size far greater than the mercury injection data will allow, or b) in some samples, given a 2 micrometer throat size, permeability is overpredicted by at least an order of magnitude. This test suggests that Pore Type 1 can support at best 0,001 - 0,003 Darcy. Pore Type 3, by virtue of small throats and low abundance, is not either a contributor to permeability.

Not surprisingly, Pore Types 2 and 4 are major contributors to permeability when assigned throat sizes coincident with the mercury porosimetry results. Pore Type 2 is most abundant in medium- to fine-grained sandstones. The abundance of Pore Type 2 is indeed positively correlated with permeability in samples in that size range. Given a throat size ranging from about 3 - 4 μm, values consistent with the mercury porosimetry), the model shows that Pore Type 2 accounts for most of the permeability in half of the samples (Table 4). That is, the large number of pores per unit area in those samples overcome the problem of relatively small throat size. A potential problem with such a pore controlling permeability values from about 0,005 to 0,100 Darcy is whether there is enough oil column to permit buoyant forces great enough for oil to penetrate Type 2 pores.

Pore Type 4 can also be a major contributor to permeability in the 0,050 - 0,100 Darcy range. At low values of permeability ($<10^{-3}$ D) the model shows that Pore Types 2 and 4 have the same throat size, indicating Type 4 pores are isolated behind clusters of Type 2 pores, either because there are too few Type 4 pores to form continuous circuits, or because they occur in clots in a bioturbated fabric dominated by Type 2 pores. At higher values of permeability, Type 4 pores are assigned a larger throat size (about 6 μm), as indicated by the mercury porosimetry results.

As discussed in the section above, Pore Type 5 possesses relatively small throats in samples with permeability values less than 0,100 D (1 to 3 μm throats). This small value is consistent with a moldic origin for Pore Type 5, they are isolated behind other

Table 4. Assignied Thoat Radii and contributions to permeability of pore types.

SAMPLE NAME	Throat Radius 1	Throat Radius 2	Throat Radius 3	Throat Radius 4	Throat Radius 5	Khat PT1	Khat PT2	Khat PT3	Khat PT4	Khat PT5	Khat PT6	Khat PT7
D36380	1,00	2,50	1,00	3,00	2,00	0,880	2,162	0,002	0,261	2,000	5,31	4,3
D36410	1,00	4,00	1,00	10,50	0,00	0,305	30,481	0,004	171,461	0,000	202,25	214
D36450	1,00	3,40	1,00	6,00	2,00	1,177	15,149	0,001	0,091	0,000	16,42	15,5
D36474	1,00	4,50	1,00	6,00	2,00	0,937	15,553	0,000	1,267	0,000	17,76	15,7
D36500	1,00	4,00	1,00	6,00	21,00	0,445	0,544	0,002	20,482	333,823	355,30	378
D36530	1,00	4,00	1,00	6,00	2,00	0,375	23,404	0,002	7,274	0,002	31,06	26,1
D36610	1,00	3,80	1,00	6,00	2,00	0,529	49,920	0,004	4,833	0,000	55,29	52,5
D36646	1,00	4,40	1,00	6,00	2,00	0,147	68,308	0,001	28,137	0,012	96,60	77,9
D36702	1,00	2,00	1,00	2,00	2,00	0,614	1,204	0,001	0,073	0,000	1,89	3,03
K06556	1,00	4,00	1,00	6,50	2,00	0,347	20,167	0,000	77,452	0,013	98,43	106,0
K06573	1,00	4,60	1,00	6,00	2,00	0.164	58,244	0,001	14,628	0,000	73,04	83,9
K06592	1,00	3,00	1,00	5,00	11,00	0.366	0,000	0,001	14,748	105,317	120,43	,107,0
K06628	0,00	3,30	1,00	6,00	2,00	0,000	6,680	0,000	1,109	0,000	7,79	6,63
K06649	1,00	3,60	1,00	3,60	2,00	0,416	0,957	0,001	1,568	0,073	3,01	2,56
K06672	1,00	4,20	1,00	5,50	2,00	0,216	9,249	0,002	15,932	0,011	25,41	25,3
K06712	1,00	4,00	1,00	5,00	6,00	0,378	12,733	0,002	10,440	0,510	24,06	25,1
K06725	1,00	2,80	1,00	6,00	2,00	0,231	6,553	0,001	15,134	0,006	21,92	23,1
K06730	1,00	2,70	1,00	5,00	2,00	0,578	10,888	0,001	2,319	0,000	13,79	11,5
K06737	1,00	3,00	1,00	3,00	2,00	0,723	1,325	0,002	0,521	0,031	2,60	1,69
K06757	1,00	3,00	1,00	5,00	2,00	0,000	21,505	0,002	9,724	0,000	31.23	32,7
K26725	1,00	0,00	1,00	9,00	2,00	0,104	0,000	0,002	124,121	0,005	124.23	119,0
K86377	1,00	4,60	1,00	6,00	2,00	0,478	91,843	0,004	0,000	0,000	92,33	
K86402	1,00	3,00	1,00	6,00	2,00	0,143	15,762	0,003	17,306	0,000	33,21	
K86409	1,00	2,80	1,00	6,00	2,00	0,736	9,161	0,001	0,000	0,000	9,90	9,75
K86438	1,00	3,80	1,00	6,00	2,00	0,971	8,160	0,000	0,679	0,000	9,81	8,54
K86471	1,00	4,00	1,00	6,00	2,00	0,400	0,000	0,001	29,805	0,033	29,52	22,5
K86494	1,00	4,30	1,00	6,00	2,00	0,190	26,743	0,001	22,878	0,007	49,82	33,0
K86521	1,00	3,00	1,00	7,00	16,00	0,237	1,091	0,002	64,437	113,774	179,54	177,0
K86535	1,00	3,00	1,00	5,00	2,00	0,000	3,656	0,005	11,203	0,043	14,91	13,2
K86551	1,00	2,70	1,00	3,00	2,00	0,081	7,069	0,001	0,760	0,003	7,91	6,71
K86578	1,00	3,50	1,00	6,00	2,00	0,000	35,611	0,000	5,616	0,000	41,23	39,4
K86582	1,00	3,00	1,00	6,00	2,00	0,565	14,891	0,001	0,000	0,000	15,46	16,4

pores. The small numbers of Pore Type 5 in most samples coupled with their small throat size means that Type 5 pores are not significant contributors to permeability for samples with less than 0,100 Darcy permeability.

However, in the most permeable samples, mercury

porosimetry indicates that Pore Type 5 forms circuits characterized by larger throats (8 to 12 μm). In these samples, also characterized by high proportions of Pore Type 5, Pore Type 5 is the dominant contributor to permeability. The enhanced throat sizes (10 - 21 μm) in Pore Type 5 in samples with the highest permeabilities (> 0,100 D) suggests that a purely moldic explanation for Type 5 pores in those samples is insupportable.

The answer lies in sample D36410, which does not contain any Pore Type 5, but its permeability modeling (see below) and the mercury injection curve suggest throats as large as 10,5 μm, the largest throat size attributed to Pore Type 4. This is strong, albeit indirect, evidence of the presence of microfractures in sample D36410. As all samples are from the same formation in the same field, it stands to reason that if one sample has been subjected to the stresses necessary to produce microfracturing, then other samples, if not all, have been subjected to the same stresses. Thus, the enhanced throat sizes for Pore Type 5 in the highest permeability samples are also probably due to microfractures.

Inspection of thin sections with the electron and petrographic microscopes indicates that grains bounding Type 5 pores are commonly extensively microfractured. These fractures are filled with the same blue-dyed epoxy resin as the pores do, and therefore cannot be an artifact of thin section preparation. The only explanation which is consistent with the petrography and physical measurements, is that enhanced permeability in the Monserrate sandstones is, in fact, due to the association of Pore Type 5 with microfractures. That is, Type 5 pores are being preferentially connected by microfractures. This suggests that regions of the sandstone fabric rich in Type 5 pores are inherently weaker (have lower fracture toughness or resistance to tensile fracturing) than fabric dominated by other pore types (Table 4). The concentration of fractures in and around large pores is consistent with theory; strain tends to accumulate around pores, unless the pores are filled with overpressured fluids which would support the rock. In the absence of overpressured fluids, strain will accumulate in the grains surrounding the larger pores, leading to microfracturing of the grains.

The permeability model adds more constraints on the estimated throat size than does the regression-based relationship between mercury injection and pore types alone. Specifically, a throat radius within a pressure bin can be estimated with the permeability modeling. Also, the sensitivity of each pore type to the measured permeability can be assessed. In many samples, pores of a given type are in such low numerical abundance that assignment of the largest throat size permitted by the mercury model will yield an infinitesimal contribution to permeability. Inspection of Table 4 will identify those samples wherein the estimated throat size is irrelevant to the permeability.

CONCLUSIONS

- Five pore types occur in the samples from the Monserrate Formation: Pore Types 1, 2 and 4 represent intergranular porosity. Mercury injection data were successfully related to pore types and associated throat sizes were determined. Pore Type 1 represents remnants of intergranular porosity and can occur in significant amounts at any grain size, but reaches maximum proportions in the finer-grained sandstones. Pore Type 3 represents intragranular porosity. It has small associated pore throats, and, like Pore Type 1, is probably a microlocation for S_{wi}. Pore Types 2 and 4 represent intergranular porosity regenerated by dissolution of carbonate cement. The latter two pore types are major controls on permeability in the 0,001 - 0,100 Darcy range, with Pore Type 4 contributing significantly in the medium-to-coarse grained sandstones. The relatively small throats associated with Pore Type 2 (3 - 4 μm) raise the possibility that such pores may lose a degree of effectiveness in the case of multi-phase flow. Pore Type 5 is moldic and has little effect on permeability in most samples. However, in some coarse grained sands-tones where Pore Type 5 is in great abundance, the fabric has been subjected to microfracturing, with the microfractures (12 - 16 μm wide) connecting the Type 5 molds into an effective porosity system increasing permeability by a factor of three or more.
- Microfracturing is not unexpected considering the tectonic setting of the Dina field. An understanding

of the mechanisms that control and localize microfracturing may aid in both exploitation of known fields and discovery of new petroleum accumulations.

REFERENCES

Bowers, M. C., Ehrlich, R. and Clark, R., 1994. "Determination of petrographic factors controlling permeability using petrographic image analysis and core data, Satun Field, Pattani Basin, Gulf of Thailand", *Marine and Petroleum Geology*, 11, (2): 148 - 156.

Bowers, M. C., Ehrlich R., Howard, J. J. and Kenyon, W. E., 1995. "Determination of porosity types from NMR data and their relationship to porosity types derived from thin section", *Jour. Petroleum Science & Eng*., 13: 1 - 14.

Carr, M. B., Ehrlich, R. , Bowers, M. C. and Howard J. J., 1996. "Correlation of porosity types derived from NMR data and thin section image analysis in a carbonate reservoir", *Jour. Petroleum Science & Eng*., 14: 115 - 131.

Ehrlich, R., Crabtree S. J., Kennedy S. K. and Cannon R. L., 1984. "Petrographic image analysis I - analysis of reservoir pore complexes", *Jour. Sed. Pet.,* 54 (4): 1.365 - 1.376.

Ehrlich, R., Horkowitz, K. O., Horkowitz, J. P. and Crabtree S. J., Jr., 1991a. "Petrography and reservoir physics I: Objective classification of reservoir porosity", *AAPG Bull.,* 75 (10): 1.547 - 1.562.

Ehrlich, R., Etris E. L., Brumfield D, Yuan L. P, and Crabtree S. J., Jr., 1991b. "Petrography and reservoir physics III: Physical models for permeability and formation factor", *AAPG Bull.,* 75 (10): 1.579 - 1.592.

Ehrlich, R., Prince, C. M. and Carr, M. B., 1997. "Sandstone reservoir assessment and production is fundamentally affected by properties of a characteristic microfabric, *SPE 38712, Annual Technical Conference Proceedings* (Oct. 5 - 8), San Antonio, Texas.

Ferm, J. B., Ehrlich, R., Kranz, R. L. and Park W. C., 1990. "The relationship between petrographic image analysis data and fracture toughness", *Bull. Assoc. Engineering Geol.*, 27 (3): 327 - 339.

Full, W. E., Ehrlich, R. and Klovan, J. E, 1981. "Extented Qmodel - Objective definition of external end members in the analysis of mixtures*", Jour. Math. Geol.,* 13 (4): 331 - 344.

Full, W. E., Ehrlich, R. and Kennedy, S. K., 1984. "Optimal configuration and information content of sets of frequency distributions", *Jour. Sed. Pet.,* 54 (1): 117 - 126.

Graton, L. C. and Fraser, H. J., 1935. "Systematic packing of spheres with particular relation to porosity and permeability", *Jour. of Geology,* 43: 785 - 909

James, R. A., 1995. "Application of petrographic image analysis to characterization of fluid-flow pathways in a highly-cemented reservoir: Kane Field, Pennsylvania, USA", *Jour. Petroleum Science & Eng*., 13 (3/4): 141-154.

McCreesh, C.A., Ehrlich, R. and Crabtree, S. J., 1991. "Petrography and reservoir physics II: Relating thin section Porosity to Capillary Pressure, the association between pore types and throat Size", *AAPG Bull.,* 75, (10): 1563 - 1578.

Prince, C. M., Ehrlich, R. and Anguy, Y., 1995. "Analysis of spatial order in sandstones II: Grain clusters, packing flaws, and the small-scale structure of sandstones", *Jour. Sed. Res.,* A65 (1): 13 - 28.